# Deciphering the complex paramagnetic NMR spectra of small laccase

Dasgupta, R.

# Chapter 6

# Dipolar dephasing for structure determination in a paramagnetic environment

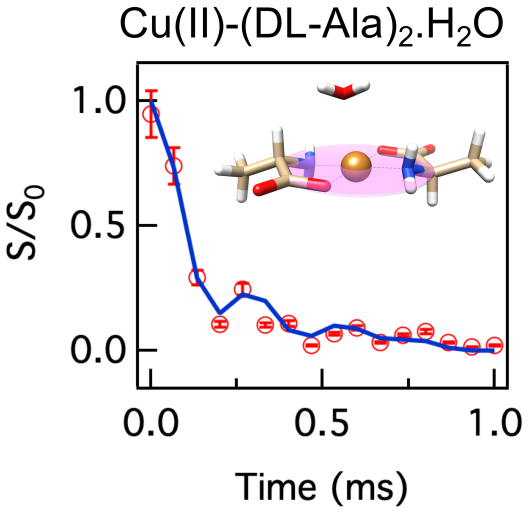


This chapter is published as:
Dasgupta, R., K.B.S.S. Gupta, D. Elam, M. Ubbink, and H.J.M. de Groot. 2021. Dipolar dephasing for structure determination in a paramagnetic environment. *Solid State Nuclear Magnetic Resonance*. 113:101728.
DOI: http://doi.org/10.1016/j.ssnmr.2021.101728

We demonstrate the efficacy of the REDOR-type sequences in determining dipolar coupling strength in a paramagnetic environment. Utilizing paramagnetic effects of enhanced relaxation rates and rapid fluctuations in Cu(II)-(DL-Ala)$_2$.$H_2O$, the dipolar coupling strength for the methyl C-H that is 4.20 Å away from the $Cu^{2+}$ ion, was estimated to be ~ 8.8 ± 0.6 kHz. This coupling is scaled by a factor of ~ 0.3 in comparison to the rigid limit value of ~ 32 kHz, in line with partial averaging of the dipolar interaction by rotational motion of the methyl group. Limited variation in the scaling factor of the dipolar coupling strength at different temperatures is observed. The C-H internuclear distance derived from dipolar coupling strength is similar to the crystal structure. The errors observed in the REDOR-type experiments are similar to those reported for diamagnetic systems. Increase in resolution due to the Fermi contact shifts, coupled with MAS frequencies of 30–35 kHz allowed to estimate the hyperfine coupling strengths for protons and carbons from the temperature dependence of the chemical shift and obtain a high resolution $^1H$–$^1H$ spin diffusion spectrum. This study shows the utility of REDOR-type sequences in obtaining reliable structural and dynamical information from a paramagnetic complex. We believe that this can help in studying the active site of metalloproteins which are paramagnetic in nature at high resolution.

## 6.1 Introduction

Paramagnetic solid-state NMR has undergone a revolution in the past decade due to the development of high spinning frequency probes and tailored pulse sequences. Studying the ligands that directly coordinate the paramagnetic metal ions with NMR can provide insight into the structure and dynamics of the system.(1–4) Among the various interactions, dipolar interactions are attractive for characterizing fast cooperative dynamics that can be measured using rotational-echo double resonance (REDOR) type solid state NMR experiments including shifted-REDOR for probing anisotropic motions.(5–7)

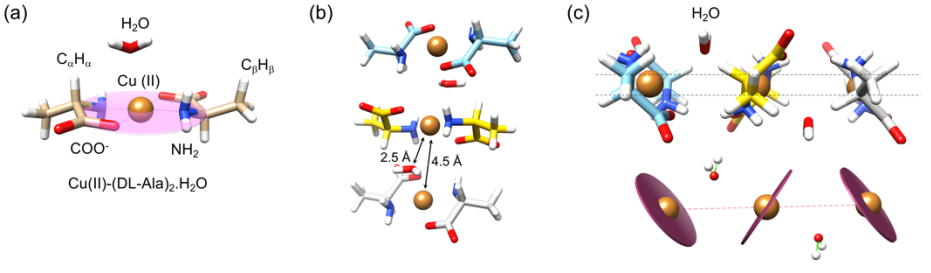

***Figure 6.1**. Cu(II)-(DL-Ala)$_2$.H$_2$O crystal structure (cif:1153761).(8) (a) Monomer depicting the plane of coordination and the respective proton and carbon orientations (b) Trimeric representation of chain with distance between copper atoms and between copper and oxygen of water and (c) Coordination plane of copper and position of water molecule.*

In this study we show that rapid paramagnetic fluctuations favorably affect REDOR and shifted REDOR experiments therefore, those can be performed with high sensitivity and resolution. We find that internuclear dipolar couplings can be determined with high accuracy that is comparable to what has been achieved for diamagnetic systems. We have selected Cu(II)-(DL-Ala)$_2$.H$_2$O (Figure 6.1) as a model system to test the utility of the REDOR type sequences and to probe the C–H dipolar coupling of the methyl group in the alanine ligand, which is directly coordinating the paramagnetic metal center.(8–11) Recently, well-resolved heteronuclear dipolar correlation spectroscopy was reported for Cu(II)-(DL-Ala)$_2$.H$_2$O.(10, 12–14) The possibility to sustain internuclear dipolar transfer in the immediate vicinity of paramagnetic ions can be attributed to rapid paramagnetic fluctuations that average the anisotropic and traceless electron-nuclear dipolar interactions while leaving the isotropic contact shifts unaffected. Here, the J-coupling between the copper ions determines the fluctuation frequencies for averaging dipolar couplings, which are traceless without isotropic component and is intrinsic to a one-dimensional chain. This results in the motional narrowing from spin waves running along the chain.(15) This opens up a window of opportunity, since essential advantages of paramagnetism, such as rapid acquisition and increased spectral dispersion can be combined with the power of dipolar correlation spectroscopy for resolving static or dynamic structure quantitatively. To demonstrate this, we implement a REDOR method for Cu(II)-(DL-Ala)$_2$.H$_2$O by adapting the REDOR refocusing period to the fast rotation needed for signal detection in paramagnetic systems with their enhanced relaxation that limits the acquisition time. The Cu(II)-(DL-Ala)$_2$.H$_2$O form 1-dimensional chains in which the $Cu^{2+}$ ions are weakly coupled.(11) The antiferromagnetic coupling $2J = -2.21$ cm$^{-1}$ translates into a characteristic frequency of ~ 70 GHz for the electronic spin fluctuations.(11) The properties of enhanced relaxation and rapid averaging of electron-nuclear dipolar interactions by paramagnetic fluctuations that are much faster than the frequency scale of the heteronuclear dipolar coupling of ~ 10 kHz or less, allow to perform heteronuclear dipolar recoupling experiments with fast MAS in a very short time, much shorter than for diamagnetic species. In addition, we show how $^1$H□$^1$H spin diffusion spectra and the temperature dependence of proton and carbon shifts from 1D Hahn-echo experiments can help to collect structural information from paramagnetic systems with ultra-fast MAS.

## 6.2 Results and discussions

### *NMR characterization of Cu(II)-(DL-Ala)$_2$.H$_2$O*

There are several advantages when working with Cu(II) paramagnetic systems. Since Cu(II) has small susceptibility the Fermi-contact interaction is stronger than the paramagnetic relaxation enhancement (PRE).(16) This results in a better resolution because of the increase in the spectral dispersion without adversely affecting the linewidth. Additionally, reduction of experimental time due to fast longitudinal relaxation compared to diamagnetic systems can be achieved. In contrast, with other metal ions such as Tb(III) the susceptibility anisotropy is large and may lead to resonances broadened beyond detection due to increase in PRE-effects.(16) Figure 6.2 shows the 1D spectra of $^{1}$H and $^{13}$C at different spinning frequencies and magnetic fields. The resolution is enhanced by the paramagnetic shifts at very fast MAS (> 20 kHz).(12–14, 17–19)

The 1D proton rotor-synchronized Hahn-echo spectra (Figure 6.2a and b) show three prominent resonances attributed to $CH_\alpha$ at 8 ppm and C**H**$_3$1 at 32 ppm and C**H**$_3$2 at 21 ppm. We observed that the intensity of C**H**$_3$1 is 4 times that of $H_\alpha$ and C**H**$_3$2, while $H_\alpha$ and C**H**$_3$2 show similar intensities. The carbon spectrum shows three prominent resonances for $C_\alpha$1 at -280 ppm, *C*O at -200 ppm and $C_\beta$1 at 180 ppm and two minor resonances for $C_\alpha$2 at -258 ppm and $C_\beta$2 at 88 ppm, (Figure 6.2c, 6.2d and Table S6.1).(10, 13, 19) The two components were attributed to two orientations of the methyl group as a consequence of crystal packing, where the major component (C**H**$_3$1/$C_\beta$1 ) is closer to the copper atom while the minor component (C**H**$_3$2/$C_\beta$2 ) is away.(8, 20) The proton signals from the $NH_2$ group (data not shown) were reported to be at -132.7 and -159.5 ppm.(10) The protons from the water molecule are generally broadened beyond detection due to fast exchange dynamics.(10, 19) The methyl group of the major component was reported to be undergoing fast rotation which results in a single resonance for the three methyl protons (Figure 6.2a and b).(10)

A dipolar-INEPT experiment was performed to check the quality of the sample and the efficiency of polarization transfer via dipolar interactions, which was previously shown to be superior to cross polarization based transfer for paramagnetic systems.(13, 21) It shows the similar spectrum (Figure 6.2d) as reported earlier albeit with better resolution and S/N allowing to identify the splitting of the methyl group response that arises due to crystal packing effects.(8, 13, 20)

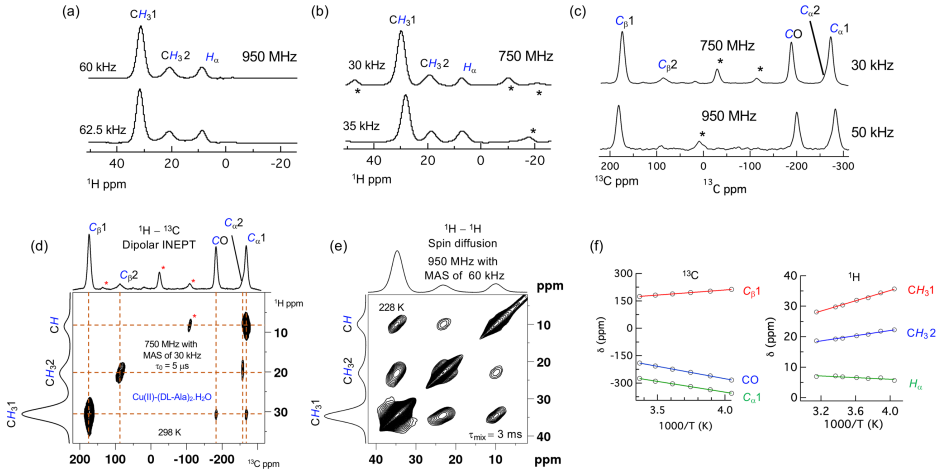


***Figure 6.2***. *(a) 1D $^{1}$H rotor synchronized Hahn-echo spectra at MAS frequencies of 60 and 62.5 kHz in an external magnetic field of 950 MHz; (b) 1D $^{1}$H rotor synchronized Hahn-echo spectra at MAS frequencies of 30 and 35 kHz in an external magnetic field of 750 MHz; (c) 1D $^{13}$C rotor synchronized Hahn-echo spectra at MAS frequencies of 30 and 50 kHz in an external magnetic field of 750 and 950 MHz respectively; (d) The 2D $^{1}$H-$^{13}$C dipolar-INEPT spectra at a MAS frequency of 30 kHz in an external magnetic field of 750 MHz with a transfer delay $\tau_0$ of 5 μs at 298 K; (e) 2D $^{1}$H-$^{1}$H spin diffusion at a MAS frequency of 60 kHz in an external magnetic field of 950 MHz with a mixing time $\tau_{mix}$ of 5 ms at 228 K; (f) Temperature dependence of the chemical shift for carbon and protons where* C**H**$_3$1 *and* $C_\beta$ *are in red,* C**H**$_3$2 *and carbonyl carbon* CO *are in blue and* $H_\alpha$ *and* $C_\alpha$ *are in green. Solid lines are the fit using equation S6.9. The spinning side bands in the upper panels are marked with asterisks. The assignments in panel (a) to (e) of $^{1}$H and $^{13}$C responses are shown in italics and blue color.*

The 2D $^{1}$H–$^{1}$H spin diffusion spectra acquired at 950 MHz with a MAS frequency of 60 kHz (Figure 6.2e and S6.3), show that a high resolution homonuclear 2D spectra can be obtained under paramagnetic conditions with modification of the pulse sequence to consider the paramagnetic effects of increased relaxation and rapid fluctuations. Similar observations were reported for copper cyclam complexes.(21)

The temperature dependence of the chemical shift shows strong Curie behavior for CO, $C_\alpha$1, $C_\beta$1, C**H**$_3$1 and C**H**$_3$2 while weak anti-Curie behavior is observed for $H_\alpha$ (Figure 6.2f and Figure S6.2a). The hyperfine coupling strengths are summarized in table 1, obtained after fitting the data with equation 9 (Figure 6.2f).(22) It is interesting to observe that, although the $H_\alpha$ is close to the copper, the hyperfine coupling constant and hence the spin density on it is less than for $H_\beta$. This was also observed in DFT calculations for Cu(II)-(DL-Ala)$_2$.H$_2$O showing very little spin density localized on the $H_\alpha$ atom.(22, 23) The sign of the hyperfine coupling strength provides

the spin polarization of the electron on the nucleus with respect to the external magnetic field. It was observed to be parallel for $C_\beta 1$, $C\mathbf{H}_3 1$ and $C\mathbf{H}_3 2$ and anti-parallel for $C_\alpha 1$, CO and $H_\alpha$ (Table 6.1 and Figure 6.2f). These observations are in line with the calculations performed on copper alanine complexes and previously reported data.(22) The estimated $\delta_{dia}$ from the fit of the temperature dependencies of the chemical shift (Figure 6.2f) is summarized in table 6.1. They differ from the expected diamagnetic chemical shift of DL-alanine (Table S6.3). This difference can be attributed to the differences in crystal packing of Cu(II)-(DL-Ala)$_2$.$H_2O$ and DL-alanine (Figure S6.6). The NMR chemical shift tensor for small molecules in solid state NMR differs significantly between different crystal forms due to changes in hydrogen bonding, stacking, ring current, C–H···π interactions etc.(24) DFT calculations of different crystal forms of purine derivatives show that the change in the diamagnetic chemical shift can be as high as 6.5 ppm, 20 ppm and 55 ppm for proton, carbon and nitrogen respectively.(24)

***Table 6.1**. Hyperfine coupling strength (A) and the estimated diamagnetic chemical shift from temperature dependencies of the resonances for carbon and protons.*

| Nuclei | *A* (MHz) | $\delta_{dia}$ (ppm) |
|---|---|---|
| $C_\alpha 1$ | -3.7 ± 0.3 | 120 ± 4 |
| $C_\beta 1$ | 1.8 ± 0.9 | -12 ± 1 |
| CO | -4.3 ± 0.4 | 265 ± 5 |
| $H_\alpha$ | -0.2 ± 0.04 | 11.0 ± 1.0 |
| $C\mathbf{H}_3 2$* | 0.5 ± 0.03 | 5.0 ± 0.9 |
| $C\mathbf{H}_3 1$* | 1.0 ± 0.03 | 1.5 ± 0.8 |

** The protons in question are indicated in bold.*

The full width at half of the maximum (FWHM) of the resonances decreases with increasing temperature (Figure S6.2b and S6.2c). Most likely, an increase in the electronic relaxation rate with temperature reduces the paramagnetic relaxation enhancement.

### *Dipolar coupling strength estimation*

Dipolar coupling measurements can provide insight into the dynamics of the molecule.(5, 25) Here, we have employed REDOR (Figure S6.4c) and shifted-REDOR (Figure S6.4d) to measure the dipolar coupling between $^1H$ and $^{13}C$ of the methyl group in Cu(II)-(DL-Ala)$_2$.$H_2O$.(5, 6) The choice of these pulse sequences was based on their robustness for amplitude mis-setting, inhomogeneities in the radiofrequency field, carrier offset and CSA.(5) The methyl group was used as a probe because of the

presence of intrinsic methyl rotation that partially averages the dipolar coupling and its higher S/N ratio compared to that of other protons (Figure 6.2a and b).

Figure 6.3a shows the $^{1}H–^{13}C$ REDOR curves of the C-H in C**H**$_3$1 group at 277 K, 287 K and 297 K obtained at a MAS frequency of 30 kHz. The dipolar coupling strengths estimated after the fitting are 8.6 kHz, 10.0 kHz and 9.2 kHz respectively (Table 6.2 and Figure 6.3b). These values correspond with a scaling factor of ~ 0.3 (Table 6.2) relative to the rigid limit value of ~ 32 kHz, consistent with previously reported data for alanine in the diamagnetic crystalline state and similar to the theoretical scaling factor of 0.333.(26) The accuracy of the paramagnetic measurement is similar to that reported for the diamagnetic systems.(5, 6)

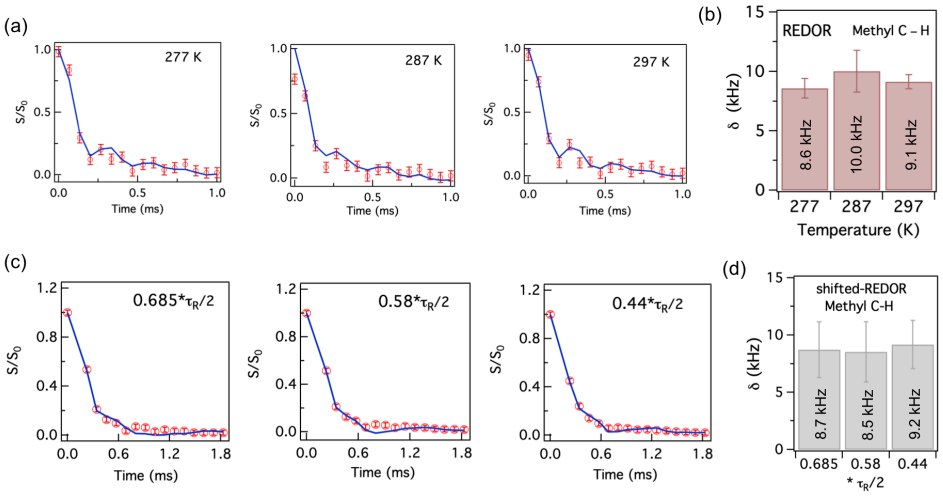


***Figure 6.3***. *(a) REDOR curve for methyl C-H (*$C_\beta$1 *and* C**H**$_3$1*) in Cu(II)-(DL-Ala)$_2$.H$_2$O at 277 K, 287 K and 297 K, the solid lines represent the fit; (b) The dipolar coupling strength estimated from fitting the REDOR curve for the methyl C-H (*$C_\beta$1 *and* C**H**$_3$1*); (c) Shifted-REDOR curves at a MAS frequency of 30 kHz with different shift of the π pulse from ideal $\tau_R/2$ (16.67 μs). The solid blue lines are fit with asymmetric parameter η value of 0.1; (d) Dipolar coupling strength estimated from the shifted-REDOR curve fit of methyl C-H (*$C_\beta$1 *and* C**H**$_3$1*).*

The corresponding internuclear $^{1}H–^{13}C$ ($C_\beta$1 and C***H***$_3$1) distances derived after dividing the dipolar coupling strength with the scaling factor is ~ 1.0 Å (Table 6.2) which is very similar to the crystal structure (1.0 Å).(8, 23) This demonstrates the efficacy of the REDOR sequence in obtaining reliable distance information in a paramagnetic system. It is noteworthy that although the paramagnetic shift is temperature dependent the dipolar coupling strength is preserved. This property can be explored to characterize the dipolar coupling strength between the nuclei in the

vicinity of the metal at the active site of the paramagnetic metalloproteins and consequently get insight into the dynamics.

***Table 6.2**. Dipolar coupling strength between C-H (*$C_\beta 1$ *and* $CH_3 1$*) at different temperatures using REDOR with a MAS frequency of 30 kHz.*

| Temp (K) | δ kHz | Scaling factor | Methyl C-H ($C_\beta 1$ and $CH_3 1$) distance (Å) |
|---|---|---|---|
| 277 | 8.6 ± 0.8 | 0.29 ± 0.03 | 1.1 ± 0.1 |
| 287 | 10.0 ± 1.7 | 0.34 ± 0.06 | 1.0 ± 0.2 |
| 297 | 9.1 ± 0.6 | 0.32 ± 0.02 | 1.0 ± 0.1 |

It was recently reported that using a variant of REDOR where the π pulses are shifted from its original position, known as shifted-REDOR (Figure S6.4d), is able to identify anisotropic motions present in the protein via the asymmetry parameter η easily by scaling down the oscillation.(5, 6) We investigated the dephasing behavior in the presence of the paramagnetic metal center at a spinning frequency of 30 kHz and at 297 K with the π pulse shift ($\tau_S$) of 0.685 or 0.58 or 0.44 times $\tau_R/2$ (Figure 6.3c). The dipolar coupling strength between the methyl C-H nuclei does not change with varying $\tau_s$ and it matches with the values obtained from REDOR (Table 6.3 and 6.4). The derived internuclear distance is ~ 1.0 Å (Table 6.3), consistent with the crystal structure and similar to REDOR. Hence, shifted-REDOR appears also robust and reliable for obtaining structural information. The asymmetry parameter η of 0.1 gave the best fit, which is in line with the lack of anisotropic motion in the methyl group rotation. While there was no anomaly in the implementation of shifted-REDOR for Cu(II)-(DL-Ala)$_2$.$H_2O$, in shifted-REDOR (Figure 6.3c), the oscillatory behavior observed in the REDOR (Figure 6.3a) is diminished which can be due to the presence of additional protons ($NH_2$ and Hα). This is consistent with the observations of Schanda *et al.* (2011), who showed that the presence of additional protons near the observed nuclei reduces the oscillatory nature of the shifted-REDOR for ubiquitin crystals.(5, 6)

***Table 6.3**. Dipolar coupling strength of methyl C-H (*$CH_3 1$*) using shifted-REDOR and at different fraction of $\tau_R/2$ by which the π pulse is shifted at MAS frequency of 35 kHz.*

| Fraction of $\tau_R/2$ shift | δ kHz | Scaling factor | Methyl C-H distance (Å) |
|---|---|---|---|
| 0.685 | 8.7 ± 2.4 | 0.30 ± 0.08 | 1.0 ± 0.3 |
| 0.580 | 8.5 ± 2.6 | 0.29 ± 0.09 | 1.1 ± 0.3 |
| 0.440 | 9.2 ± 2.1 | 0.32 ± 0.07 | 1.0 ± 0.2 |

In summary, both REDOR and shifted-REDOR sequences provide reliable estimates of the dipolar coupling strength and consequently information about the structure and methyl rotation.

## 6.3 Conclusions

This study shows that high resolution $^{1}H$ based solid-state NMR spectra can be obtained for a paramagnetic system at fast MAS (> 25 kHz). Using the high sensitivity of $^{1}H$ and the high resolution due to the paramagnetic nature of Cu(II), a temperature dependence study of the model compound Cu(II)-(DL-Ala)$_2$.$H_2O$ could be performed that shows that the shift correlates with the spin delocalization over the ligands. The fast MAS has enabled the implementation of $^{1}H$–$^{1}H$ homonuclear spin diffusion, REDOR and shifted-REDOR pulse sequences. Our benchmark is the existing crystal structure. The error in the measured values were similar to that observed for diamagnetic systems and are largely systematic errors from e.g. thermal motions that effectively reduce the dipolar coupling from its rigid limit value. We present a technical step forward by showing that both REDOR and shifted-REDOR are quantitatively reliable in determining the dipolar coupling strength and internuclear distances near the paramagnetic metal center, which paves the way for future application in metalloproteins to probe fast dynamics. In addition, the results contribute to the converging and convincing evidence that paramagnetic solid-state NMR is increasingly accessible and can be interpreted in the same way as the NMR spectra of diamagnetic solids.

# 6.4 Supporting Information

### *Sample preparation and solid-state NMR experiments*

Cu(II)-(DL-Ala)$_2$.H$_2$O complex was synthesized as reported earlier.(10) All chemicals including the uniformly labelled $^{13}$C-DL-alanine were obtained from Sigma Aldrich (USA).

Solid-state NMR experiments were performed with AV-I (17.6 T) 750 MHz and AV-HDIII (22.31 T) 950 MHz spectrometers equipped with a 2.5 mm and 1.3 mm MAS probe, respectively, at spinning frequencies ranging from 30 to 62.5 kHz. 1D proton and carbon spectra were recorded with a rotor synchronized Hahn-echo sequence (Figure S6.4a). The high-power $\pi/2$ pulses were 2 μs and 2.5 μs for $^1$H and $^{13}$C, respectively. A dead time of 4.5 μs was subtracted from the refocusing period in the Hahn-echo pulse sequence. A comparison of spectra obtained with single 90$^o$ pulse (Figure S6.1) with rotor synchronized Hahn-echo spectra (Figure 6.2) confirms that there is little phase distortion in echo spectra obtained with a large spectral window (SW).(4) The advantage of using rotor-synchronized Hahn-echo over single 90$^o$ pulse is elimination of probe artifacts as observed from Figure S6.1a and Figure 6.2a. This prompted us to use rotor-synchronized Hahn-echo pulse sequence to obtain 1D spectra for both carbon and proton for further study.

The 1D and 2D dipolar-INEPT sequence was adopted from Wickramasinghe *et al*., (2008) with a $\pi/2$ pulse length similar to the rotor synchronized Hahn-echo experiment.(13) Temperature dependent experiments were performed at temperatures between 247 K and 318 K. For the 2D $^1$H–$^1$H spin diffusion (Figure S6.4b) experiment the mixing time was varied from 1 ms to 5 ms with a total acquisition time of 530 μs and a delay of 30 ms between scans. 200 slices of data were acquired in the t1 dimension in a total experiment time of < 5 mins. REDOR and shifted-REDOR data were collected by direct excitation of $^{13}$C (Figure S6.4c and S6.4d).(5, 6)·(27–29) The $\pi/2$ pulse lengths were 2 μs and 2.2 μs for $^1$H and $^{13}$C respectively. Temperature calibration was done using samarium tin oxide and lead nitrate.(30–32) Data analysis was performed with TOPSPIN 4.0.5 (Bruker) and Igor pro 6.37.

### *REDOR and shifted-REDOR data analysis*

The REDOR and shifted-REDOR curves were fitted with SIMPSON 4.2.1.(33, 34) The geometry of Cu(II)-(DL-Ala)$_2$.H$_2$O was adopted from Calvo *et al*., and Zhang *et al*., to generate the spin system parameters, dipolar coupling and Euler angles using SIMMOL-VMD.(8, 23, 35, 36) The signal from the methyl C-H was used as a reporter to determine the dipolar coupling strength due to its intrinsic isotropic motion and

high S/N ratio (Figure 6.2a and b). The fitting algorithm as implemented in SIMPSON package was used to estimate the dipolar coupling.(33–35)

The rigid limit dipolar coupling strength of the methyl C-H is ~ 32.1 kHz which corresponds to an internuclear distance of 0.98 Å.(23) It is known that methyl rotation partially averages the dipolar coupling between the C-H bond of the methyl group and therefore the rigid limit dipolar coupling is scaled according to(26, 37)

$$D_{avg} = S * D, \tag{S6.1}$$

with $D$ being the dipolar coupling strength in the rigid limit. The scaling factor is

$$S = (3cos^2\theta - 1)/2, \tag{S6.2}$$

where $\theta$ is the angle between the methyl C-H and the rotational axis, which in this case is the bond between $C_\alpha - C_\beta$. For a tetrahedral geometry of the methyl group $\theta$ = 109.5°. This gives a theoretical scaling factor of $S$ = 0.333 (Figure S6.5) and $D_{avg}$=10.69 kHz for the C-H bond in Cu(II)-(DL-Ala)$_2$.H$_2$O in the rotating methyl group. For the analysis of the data, the scaled $D_{avg}$ = 10.69 kHz was changed to fit the experimental data. The average dipolar coupling strength was optimized to fit the REDOR curve using the fitting algorithm of SIMPSON. The homonuclear dipolar coupling between the three protons of the methyl group was also scaled by the theoretical value of 0.333 to give a $D_{avg}$ = 9.76 kHz.(23) The codes for fitting and to obtain the spin-system are uploaded in https://github.com/rubindg/REDOR_fitting_simpson.

### *Theory of temperature dependence of Fermi contact shifted resonances*

The chemical shift of the paramagnetic system is temperature dependent and the observed chemical shift is given by (16)

$$\delta_{obs} = \delta_{dia} + \delta_{FCS} + \delta_{PCS}, \tag{S6.3}$$

where $\delta_{dia}$ is the diamagnetic chemical shift and $\delta_{CS}$, $\delta_{PCS}$ are the contributions from the Fermi contact shift (FCS) and pseudo-contact shift (PCS) respectively.(16, 38) For the nuclei of coordinating ligands FCS >> PCS and eq. 1 can be written as

$$\delta_{obs} \approx \delta_{dia} + \delta_{FCS}. \tag{S6.4}$$

The contribution from the FCS is given by(38)

$$\delta_{FCS} = \frac{A\langle S_z\rangle}{\hbar\gamma_I B_0}, \tag{S6.5}$$

with $A = \frac{2}{3}\hbar\gamma_I\mu_B g_e\mu_0\rho$ the isotropic hyperfine coupling that is proportional to the spin density $\rho$ on a nucleus. The $\langle S_z\rangle$ is the expectation value of the $z$ magnetization, $\hbar$ is

the reduced Planck constant, $\gamma_I$ is the gyromagnetic ratio of the nucleus in question, and $B_0$ is the external magnetic field.
Since the $\langle S_z \rangle$ is related to the magnetic susceptibility according to(38, 39)

$$\langle S_z \rangle = \frac{B_0 \chi}{\mu_B g_e \mu_0}, \quad \text{(S6,6)}$$

where $\mu_B$ is the Bohr magneton, $g_e \approx 2.003$ is the free electron $g$-value, and $\mu_0$ is the permeability of the vacuum, the FCS can also be expressed in terms of the magnetic susceptibility $\chi$ by

$$\delta_{FCS} = \frac{A\chi}{\hbar \gamma_I \mu_B g_e \mu_0}. \quad \text{(S6.7)}$$

The system is a linear chain in the high temperature limit, since $2J = -2.2$ cm$^{-1}$, which translates into ~ 3 K. Therefore, we are in the high temperature limit, $|2J| \ll T$, and the experiments for Cu(II)-(DL-Ala)$_2$.H$_2$O were performed at this limit. The magnetic susceptibility is given by(40)

$$\chi = \frac{S(S+1)\mu_B^2 g_e^2 \mu_0}{3k_B T}, \quad \text{(S6.8)}$$

where $S = 1/2$ is the spin of the Cu(II) ion, $k_B$ is the Boltzmann constant and $T$ is the temperature in Kelvin. Substituting eq. 6 in eq. 5, and in eq. 2 we obtain

$$\delta_{obs} \approx \delta_{dia} + A\frac{S(S+1)\mu_B g_e}{3\hbar \gamma_I k_B T} \quad \text{(S6.9)}$$

for the temperature dependent chemical shift, which was used to determine hyperfine couplings and spin densities by fitting to the data in Figure 6.3.

## *Supporting figures and tables*

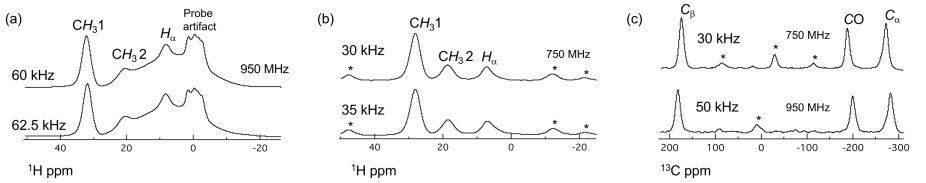


***Figure S6.1***. *Single 90° pulse experiment for $^{1}H$ at (a) 950 MHz with MAS of 60 kHz and 62.5 kHz, (b) 750 MHz at MAS of 30 kHz and 35 kHz and for $^{13}C$ at (c) 750 MHz with MAS of 30 kHz and 950 MHz with MAS of 50 kHz. Resonances marked with * are the spinning side bands. $^{1}H$ and $^{13}C$ assignments are indicated with italics.*

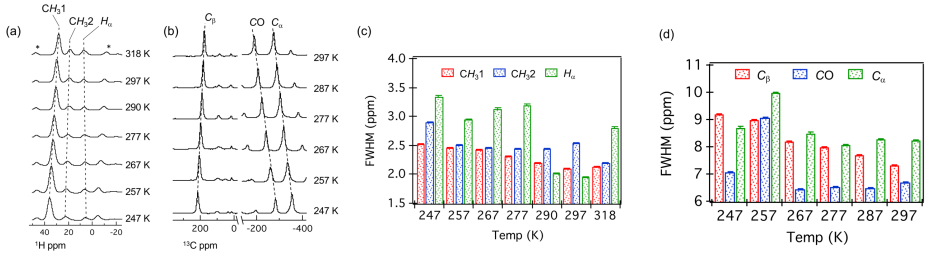


***Figure S6.2.*** *Temperature dependence of (a) Proton and (b) Carbon signals at 30 kHz MAS in a magnetic field of 14 T. The full width at half of the maximum FWHM of (c) Protons (red = C**H**$_3$1, blue = C**H**$_3$2 and green = H$_\alpha$) and (d) Carbons (red = C$_\beta$, blue = CO and green = C$_\alpha$) at different temperature. The peaks marked with stars are the spinning side bands while the smaller peaks in carbon spectra are from small impurities and spinning side bands. Assignments of $^{1}H$ and $^{13}C$ signals are indicated in italics.*

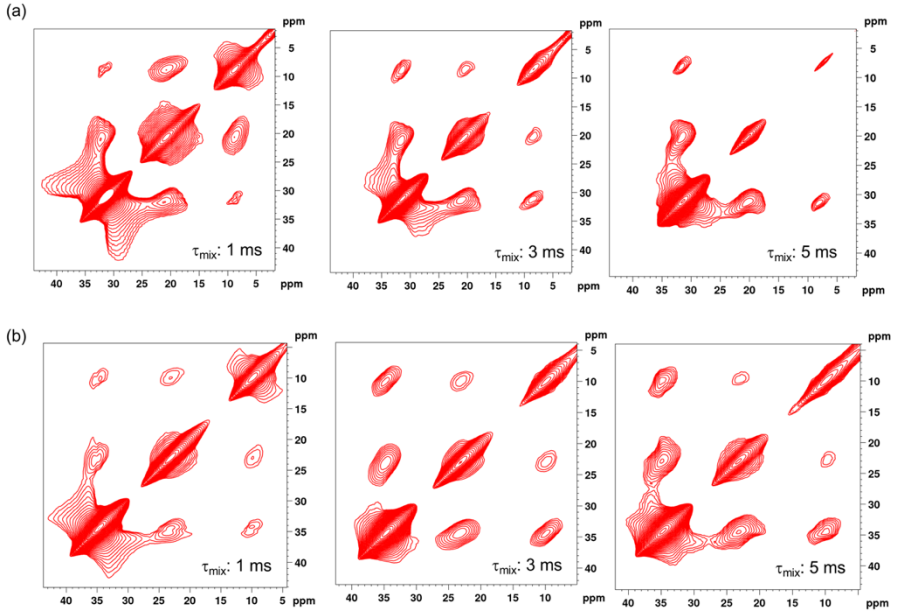


***Figure S6.3.*** *$^{1}$H–$^{1}$H spin diffusion spectra at (a) 300 K and (b) 228 K at 60 kHz MAS and 950 MHz $^{1}$H frequency with mixing times of 1 ms, 3 ms and 5 ms.*

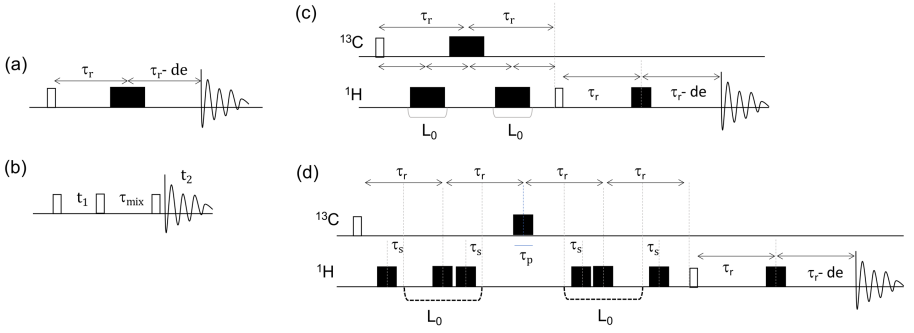


***Figure S6.4.*** *Pulse sequences used in this study. (a) Rotor synchronized Hahn-echo, (b) $^{1}$H–$^{1}$H spin diffusion, (c) Proton detected standard REDOR and (d) Proton detected shifted-REDOR. $\tau_r$ denotes the rotor period, $t_1$ and $t_2$ are the two-time domains for 2D spectra, $\tau_s$ is (0.68 to 0.44)* $\tau_R/2$, $\tau_p$ is the $\pi$ pulse length, de is the dead time of the instrument, $\tau_{mix}$ is the mixing time and $L_0$ is the loop counter for repeating the $\pi$ pulses.*

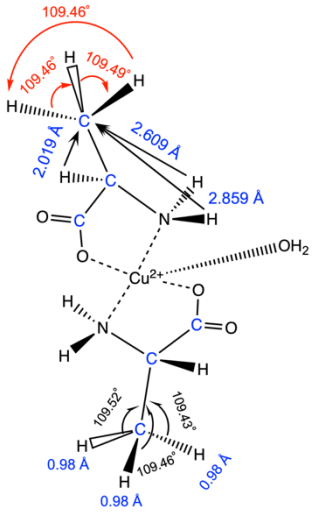


***Figure S6.5***. *Geometry of Cu(II)-(DL-Ala)2.H₂O adopted from Zhang et al.,(23)*

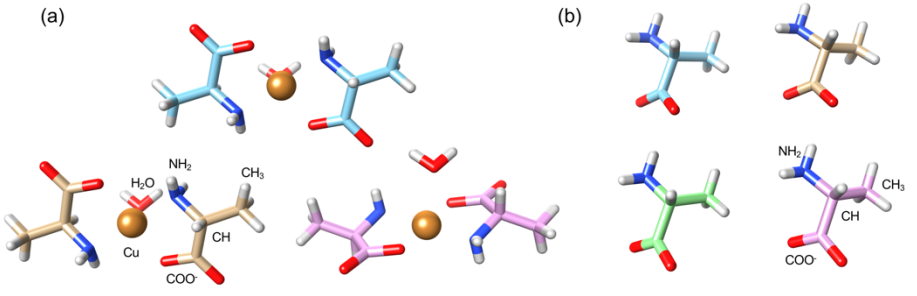


***Figure S6.6.*** *Crystal packing in a unit cell of (a) Cu(II)-(DL-Ala)₂.H₂O (cif:1153761)(8) and (b) DL-alanine (cif:164668)(41).*

***Table S6.1**. Assignment of $^{1}H$ spectra from the literature on Cu(II)-(DL-Ala)$_2$.H$_2$O.(10, 19) The magnetic field used was from 7.5 T to 11.75 T with spinning frequencies between 15 and 30 kHz.*

| Protons of group | $\delta_{iso}$ (ppm) |
|---|---|
| $CH_3$ | 32 & 20.4 |
| CH | 8.4 |
| $NH_2$ | -132.7 & -159.5 |
| $H_2O$ | 1 |

***Table S6.2**. Properties of Cu(II)-(DL-Ala)$_2$.H$_2$O experimentally determined.*

| Properties | | Reference |
|---|---|---|
| Intrachain AFM exchange coupling constant $2J_0$ at T > 1.8 K | -2.27 ± 0.08 cm$^{-1}$ | (11) |
| g-factor | 2.091 ± 0.005 | (11) |
| Curie temperature from NMR | 6.5 K | (20) |
| Curie Temperature from $\chi_M$ (T) vs log T | 2.1 K | (8) |
| $^{13}C$ $T_1\rho$ @ 344 K | ms | (17) |
| *C*O | 8.7 ± 0.1 | |
| *C*H | 13.9 ± 0.3 | |
| *C*H$_3$ | 50.4 ± 1.9 | |
| $\Delta_{aniso}$ @ 297 K | ppm | (17) |
| *C*O | -331 ± 4 | |
| *C*H | -149 ± 10 | |
| *C*H$_3$ | 53 ± 2 | |

* The $^{13}C$ assignments are indicated in italics.

## 6.5 References


1. Pintacuda, G., N. Giraud, R. Pierattelli, A. Böckmann, I. Bertini, and L. Emsley. 2007. Solid-State NMR Spectroscopy of a Paramagnetic Protein: Assignment and Study of Human Dimeric Oxidized CuII–ZnII Superoxide Dismutase (SOD). *Angewandte Chemie International Edition*. 46:1079–1082.
2. Bertini, I., L. Emsley, M. Lelli, C. Luchinat, J. Mao, and G. Pintacuda. 2010. Ultrafast MAS Solid-State NMR Permits Extensive 13C and 1H Detection in Paramagnetic Metalloproteins. *J. Am. Chem. Soc.* 132:5558–5559.
3. Gwendal Kervern, †, † Guido Pintacuda, ‡ Yong Zhang, ‡ Eric Oldfield, § Charbel Roukoss, § Emile Kuntz, ‖ Eberhardt Herdtweck, § Jean-Marie Basset, † Sylvian Cadars, † Anne Lesage, § and Christophe Copéret, and † Lyndon Emsley*. 2006. Solid-State NMR of a Paramagnetic DIAD-FeII Catalyst: Sensitivity, Resolution Enhancement, and Structure-Based Assignments.
4. Pell, A.J., and G. Pintacuda. 2015. Broadband solid-state MAS NMR of paramagnetic systems. *Progress in Nuclear Magnetic Resonance Spectroscopy*. 84–85:33–72.
5. Schanda, P., B.H. Meier, and M. Ernst. 2011. Accurate measurement of one-bond H–X heteronuclear dipolar couplings in MAS solid-state NMR. *Journal of Magnetic Resonance*. 210:246–259.
6. Schanda, P., M. Huber, J. Boisbouvier, B.H. Meier, and M. Ernst. 2011. Solid-State NMR Measurements of Asymmetric Dipolar Couplings Provide Insight into Protein Side-Chain Motion. *Angew. Chem. Int. Ed.* 50:11005–11009.
7. Jain, M.G., K.R. Mote, J. Hellwagner, G. Rajalakshmi, M. Ernst, P.K. Madhu, and V. Agarwal. 2019. Measuring strong one-bond dipolar couplings using REDOR in magic-angle spinning solid-state NMR. *J. Chem. Phys.* 150:134201.
8. Calvo, R., P.R. Levstein, E.E. Castellano, S.M. Fabiane, O.E. Piro, and S.B. Oseroff. 1991. Crystal structure and magnetic interactions in bis (D, L-alaninato) copper (II) hydrate. *Inorganic chemistry*. 30:216–220.
9. Mirceva, A., J.O. Thomas, and T. Gustafsson. 1989. Structure of trans-bis(dl-α-alaninato)copper(II) monohydrate. *Acta Cryst C, Acta Cryst Sect C, Acta Crystallogr C, Acta Crystallogr Sect C, Acta Crystallogr C Cryst Struct Commun, Acta Crystallogr Sect C Cryst Struct Commun*. 45:1141–1144.
10. Liu, K., D. Ryan, K. Nakanishi, and A. McDermott. 1995. Solid state NMR studies of paramagnetic coordination complexes: A comparison of protons and deuterons in detection and decoupling. *J. Am. Chem. Soc.* 117:6897–6906.
11. Calvo, R., R.P. Sartoris, H.L. Calvo, E.F. Chagas, and R.E. Rapp. 2016. Antiferromagnetic spin chain behavior and a transition to 3D magnetic order in Cu(D,L-alanine)2: Roles of H-bonds. *Solid State Sciences*. 55:144–151.
12. Ishii, Y., N.P. Wickramasinghe, and S. Chimon. 2003. A New Approach in 1D and 2D $^{13}C$ High-Resolution Solid-State NMR Spectroscopy of Paramagnetic Organometallic Complexes by Very Fast Magic-Angle Spinning. *J. Am. Chem. Soc.* 125:3438–3439.
13. Wickramasinghe, N.P., and Y. Ishii. 2006. Sensitivity enhancement, assignment, and distance measurement in 13C solid-state NMR spectroscopy for paramagnetic systems under fast magic angle spinning. *Journal of Magnetic Resonance*. 181:233–243.
14. Ishii, Y., and N.P. Wickramasinghe. 2008. 1H and 13C High-Resolution Solid-State NMR of Paramagnetic Compounds Under Very Fast Magic Angle Spinning. In: Modern Magnetic Resonance. Springer, Dordrecht. pp. 467–474.
15. Kolbert, A.C., R. Verel, H.J.M. de Groot, and M. Almeida. 1997. Determination of the spin density distribution in the organic conductor DMTM(TCNQ)2 with 13C magic angle spinning NMR. *Molecular Physics*. 91:725–730.
16. Bertini, I., C. Luchinat, G. Parigi, and E. Ravera. 2017. NMR of paramagnetic molecules: applications to metallobiomolecules and models. Second edition. Amsterdam: Elsevier.
17. Wickramasinghe, N.P., M.A. Shaibat, C.R. Jones, L.B. Casabianca, A.C. de Dios, J.S. Harwood, and Y. Ishii. 2008. Progress in C13 and H1 solid-state nuclear magnetic resonance for paramagnetic systems under very fast magic angle spinning. *The Journal of Chemical Physics*. 128:052210.

18. Wickramasinghe, N.P., M. Shaibat, and Y. Ishii. 2005. Enhanced Sensitivity and Resolution in 1H Solid-State NMR Spectroscopy of Paramagnetic Complexes under Very Fast Magic Angle Spinning. *J. Am. Chem. Soc.* 127:5796–5797.
19. Willans, M.J., D.N. Sears, and R.E. Wasylishen. 2008. The effectiveness of 1H decoupling in the 13C MAS NMR of paramagnetic solids: An experimental case study incorporating copper(II) amino acid complexes. *Journal of Magnetic Resonance*. 191:31–46.
20. Sandreczki, T., D. Ondercin, and R.W. Kreilick. 1979. Low-temperature NMR studies of a single crystal of trans-Cu(DL-ala)2.H2O. *J. Am. Chem. Soc.* 101:2880–2884.
21. Kumara Swamy, S.K., A. Karczmarska, M. Makowska-Janusik, A. Kassiba, and J. Dittmer. 2013. Solid-State NMR Correlation Experiments and Distance Measurements in Paramagnetic Metalorganics Exemplified by Cu-Cyclam. *ChemPhysChem*. 14:1864–1870.
22. Szalontai, G., R. Csonka, G. Speier, J. Kaizer, and J. Sabolović. 2015. Solid-State NMR Study of Paramagnetic Bis(alaninato-κ $^{2}$ *N* , *O* )copper(II) and Bis(1-amino(cyclo)alkane-1-carboxylato-κ $^{2}$ *N* , *O* )copper(II) Complexes: Reflection of Stereoisomerism and Molecular Mobility in $^{13}$ C and $^{2}$ H Fast Magic Angle Spinning Spectra. *Inorganic Chemistry*. 54:4663–4677.
23. Zhang, Y., H. Sun, and E. Oldfield. 2005. Solid-State NMR Fermi Contact and Dipolar Shifts in Organometallic Complexes and Metalloporphyrins. *J. Am. Chem. Soc.* 127:3652–3653.
24. Babinský, M., K. Bouzková, M. Pipíška, L. Novosadová, and R. Marek. 2013. Interpretation of Crystal Effects on NMR Chemical Shift Tensors: Electron and Shielding Deformation Densities. *J. Phys. Chem. A*. 117:497–503.
25. Schanda, P., and M. Ernst. 2016. Studying dynamics by magic-angle spinning solid-state NMR spectroscopy: Principles and applications to biomolecules. *Progress in Nuclear Magnetic Resonance Spectroscopy*. 96:1–46.
26. Wu, C.H., B.B. Das, and S.J. Opella. 2010. 1H–13C hetero-nuclear dipole–dipole couplings of methyl groups in stationary and magic angle spinning solid-state NMR experiments of peptides and proteins. *Journal of Magnetic Resonance*. 202:127–134.
27. Jaroniec, C.P., B.A. Tounge, C.M. Rienstra, J. Herzfeld, and R.G. Griffin. 2000. Recoupling of Heteronuclear Dipolar Interactions with Rotational-Echo Double-Resonance at High Magic-Angle Spinning Frequencies. *Journal of Magnetic Resonance*. 146:132–139.
28. Schaefer, J. 2011. "Development of REDOR rotational-echo double-resonance NMR" by Terry Gullion and Jacob Schaefer [J. Magn. Reson. 81 (1989) 196–200]. *Journal of Magnetic Resonance*. 213:421–422.
29. Gertman, R., I. Ben Shir, S. Kababya, and A. Schmidt. 2008. In Situ Observation of the Internal Structure and Composition of Biomineralized Emiliania huxleyi Calcite by Solid-State NMR Spectroscopy. *J. Am. Chem. Soc.* 130:13425–13432.
30. Aliev, A.E., and K.D.M. Harris. 1994. Simple technique for temperature calibration of a MAS probe for solid-state NMR spectroscopy. *Magn. Reson. Chem.* 32:366–369.
31. Guan, X., and R.E. Stark. 2010. A general protocol for temperature calibration of MAS NMR probes at arbitrary spinning speeds. *Solid State Nuclear Magnetic Resonance*. 38:74–76.
32. Langer, B., I. Schnell, H.W. Spiess, and A.-R. Grimmer. 1999. Temperature Calibration under Ultrafast MAS Conditions. *Journal of Magnetic Resonance*. 138:182–186.
33. Bak, M., J.T. Rasmussen, and N.C. Nielsen. 2000. SIMPSON: A General Simulation Program for Solid-State NMR Spectroscopy. *Journal of Magnetic Resonance*. 147:296–330.
34. Tošner, Z., R. Andersen, B. Stevensson, M. Edén, N.Chr. Nielsen, and T. Vosegaard. 2014. Computer-intensive simulation of solid-state NMR experiments using SIMPSON. *Journal of Magnetic Resonance*. 246:79–93.
35. Vosegaard, T., A. Malmendal, and N.C. Nielsen. 2002. The Flexibility of SIMPSON and SIMMOL for Numerical Simulations in Solid-and Liquid-State NMR Spectroscopy. *Monatshefte für Chemie*. 133:1555–1574.
36. Bak, M., R. Schultz, T. Vosegaard, and N.Chr. Nielsen. 2002. Specification and Visualization of Anisotropic Interaction Tensors in Polypeptides and Numerical Simulations in Biological Solid-State NMR. *Journal of Magnetic Resonance*. 154:28–45.
37. Asami, S., and B. Reif. 2019. Accessing Methyl Groups in Proteins via 1 H-detected MAS Solid-state NMR Spectroscopy Employing Random Protonation. *Scientific Reports*. 9:1–13.
38. Bertini, I., C. Luchinat, and G. Parigi. 2002. Magnetic susceptibility in paramagnetic NMR. *Progress in Nuclear Magnetic Resonance Spectroscopy*. 40:249–273.

39. La Mar, G.N., G.R. Eaton, R.H. Holm, and F.Ann. Walker. 1973. Proton magnetic resonance investigation of antiferromagnetic oxo-bridged ferric dimers and related high-spin monomeric ferric complexes. *J. Am. Chem. Soc.* 95:63–75.
40. Sinn, E. 1970. Magnetic exchange in polynuclear metal complexes. *Coordination Chemistry Reviews*. 5:313–347.
41. Subha Nandhini, M., R.V. Krishnakumar, and S. Natarajan. 2001. dl-Alanine. *Acta Cryst C*. 57:614–615.